Lasers in Medical Science (2019) 34:1207–1215
https://doi.org/10.1007/s10103-018-02711-2

ORIGINAL ARTICLE

Pattern analysis of 532- and 1064-nm microlens array-type, picosecond-domain laser-induced tissue reactions in ex vivo human skin

Hye Jin Chung[1] · Hee Chul Lee[2] · Jinyoung Park[2] · James Childs[3] · Jumi Hong[2] · Heesu Kim[4] · Sung Bin Cho[4,5]

Received: 11 November 2018 / Accepted: 21 December 2018 / Published online: 2 January 2019

Abstract

Optical pulses from picosecond lasers can be delivered to the skin using microlens array (MLA) optics or a diffractive beam splitter to generate multiple, focused, high-intensity, micro-injury zones in the epidermis and dermis. The aim of our study was to histopathologically and immunohistochemically evaluate the patterns of 532- and 1064-nm MLA-type, picosecond laser-induced tissue reactions in human skin immediately after treatment. Picosecond neodymium:yttrium–aluminum–garnet (Nd:YAG) laser treatment using an MLA-type beam at the wavelengths of 532 nm and 1064 nm was delivered ex vivo to human skin. Irradiated skin specimens were then microscopically analyzed after hematoxylin and eosin staining and CD31 and Melan-A immunostaining. A single pulse of 532-nm MLA-type, picosecond laser treatment elicited cystic cavitation lesions at sizes of 83.4 ± 16.5 μm × 70.2 ± 17.3 μm (31-mm distance step) and 91.0 ± 44.7 μm × 81.2 ± 36.3 μm (48-mm distance step) in the epidermis and papillary dermis. Meanwhile, a single pulse of 1064-nm laser treatment generated cystic cavitation lesions at sizes of 107.0 ± 18.1 μm × 83.3 ± 37.4 μm (single-pulse mode) and 100.8 ± 40.4 μm × 83.1 ± 29.4 μm (dual-pulse mode) throughout the lower epidermis and upper papillary dermis. Lining epithelial cells in cystic cavitation lesions in the epidermis showed Melan-A-positive immunoreactivity, while cystic cavitation lesions in the dermis exhibited CD31-positive or CD31-negative/Melan-A-negative immunoreactivity. The present data can be used to predict 532- and 1064-nm MLA-type, picosecond-domain laser-induced tissue reactions in human skin.

Keywords Laser · Neodymium-doped yttrium–aluminum–garnet · Picosecond · Human skin · Pigment · Laser-induced tissue breakdown

Introduction

Microlens array (MLA) optics or diffractive beam splitters have been adopted to picosecond-domain lasers to generate multiple focused, high-intensity, micro-injury zones in the epidermis and dermis [1]. These micro-injury zones present histologically as intraepidermal and upper dermal vacuoles: the numbers and sizes of the vacuoles appear to depend on the melanin index of the skin and the picosecond laser energy settings [2, 3]. In addition to the initiation of wound repair processes in irradiated dermal tissue, intraepidermal laser-induced tissue breakdown also promotes the secretion of cytokines and chemokines from keratinocytes to stimulate new collagen, elastin, and mucin production for dermal remodeling [4–6]. Thereby, picosecond laser-induced, high-intensity, micro-injury zones have been shown to clinically improve skin texture, atrophic scars, and wrinkles [2, 4, 7].

For generating "seed" electrons, multiphoton absorption has a higher irradiation threshold (~ 10^{13} W/cm^2 in water) than thermionic emission [8]. Thermionic emission, however, has a lower irradiation threshold and is affected much more by the absorption properties of chromophores in target tissue, compared to multiphoton absorption [8]. In in vivo human skin,

Hye Jin Chung and Hee Chul Lee contributed equally to this work.

✉ Sung Bin Cho
drsbcho@gmail.com

[1] Department of Dermatology, Boston University School of Medicine, Boston, MA, USA

[2] R&D Center, Lutronic Corporation, Goyang, Republic of Korea

[3] Global Center, Lutronic Corporation, Billerica, MA, USA

[4] Department of Dermatology and Cutaneous Biology Research Center, International St. Mary's Hospital, Catholic Kwandong University College of Medicine, 25 Simgok-ro, Seo-gu, 22711 Incheon, Republic of Korea

[5] Kangskin Dermatology Clinic, Seoul, Republic of Korea

chromophore-dependent tissue breakdown shows more and larger microscopic vacuoles in skin with a higher melanin index [1, 3]. Multiphoton microscopy images have revealed that laser-induced tissue breakdown begins upon absorption of picosecond laser energy primarily by pigmented chromophores [1]. Nonetheless, the precise initiation mechanism of producing seed electrons for tissue breakdown by picosecond laser treatment in Asian skin of a high melanin index still remains to be elucidated.

The initiation mechanism of picosecond-laser-induced tissue breakdown begins from the production of free seed electrons by a laser pulse via multiphoton absorption or thermionic emission [8]. Thereafter, the density of electrons increases to form a plasma at the focal area, which additionally absorbs the remaining energy of the laser pulse quite efficiently [2]. The plasma then expands at a supersonic velocity and drives a shock wave. Finally, the shock-wave expansion of vaporized materials creates cavitation bubbles that further expand outward to the co-located tissue to generate microscopic vacuolar tissue reactions [2].

In this observational descriptive study, we evaluated the patterns of tissue reactions induced by 532- and 1064-nm MLA-type, picosecond, neodymium:yttrium–aluminum–garnet (Nd:YAG) laser treatment in ex vivo human skin. To do so, picosecond-domain laser treatments at the wavelengths of 532 and 1064 nm were performed on the ex vivo tissue samples of an Asian patient using an MLA-type beam. We also compared patterns of tissue reactions elicited with different distance step settings between the microlens and the skin, as well as between single-pulse and dual-pulse modes. For further investigation, the specimens were evaluated following CD31 and Melan-A immunostaining.

Materials and methods

Laser devices

A 532- and 1064-nm picosecond-domain, Nd:YAG laser device (PICOPLUS; Lutronic Corp., Goyang, Korea) with a pulse duration of 450 ps (psec) was used in this study. This device employs a master oscillator power amplifier configuration to maintain a constant pulse width, regardless of output fluence [9]. With appropriate optics, the laser energy can be delivered to target tissue as a single flat-top beam or an MLA-type beam according to therapeutic purposes. With an MLA-type optic array, a single pulse of picosecond laser energy comprised 314 microbeams at a 10-mm spot size, 154 microbeams at a 7-mm spot size, 113 microbeams at a 6-mm spot size, and 50 microbeams at a 4-mm spot size. The distances between the microlens and the surface of the skin can be regulated at 31 mm (microbeam size, 150 μm), 33 mm (microbeam size, 160 μm), and 48 mm (microbeam size, 300 μm). Furthermore, a single-pulse or a dual-pulse mode can be utilized to deliver the laser energy: the dual-pulse mode comprises two consecutive, half-fluenced, 450-ps pulses at 1.5-ns intervals.

Preparation of ex vivo human skin and laser treatment

This study was approved by the Institutional Review Board of International St. Mary's Hospital, Catholic Kwandong University College of Medicine. After obtaining written informed consent, human skin samples were obtained from one abdominoplasty surgery procedure (54-year-old Korean female with Fitzpatrick skin type III) in order to histopathologically and immunohistochemically evaluate the patterns of immediate tissue reactions of 532- and 1064-nm MLA-type, picosecond laser treatment in an ex vivo human skin model. A total of two skin samples of 10 cm × 10 cm in size was prepared; the skin samples were subsequently marked with black ink to outline 1-cm^2 grids for each experimental setting (a total of 72 grids). Each grid was placed at least 0.5 cm from the others to minimize picosecond-domain laser-induced photothermal and photoacoustic effects on the other areas.

Immediately after obtaining the ex vivo human skin samples, all experiments were performed in triplicate, and the temperature of samples was maintained between 34 and 36 °C on a heat plate during the experiments. Using an MLA-type handpiece, picosecond Nd:YAG laser treatments at the wavelength of 532 nm were performed separately on each grid with a spot size of 6 mm and a laser fluence of 1.0 J/cm^2 over a single pass at the distance steps of 31 mm and 48 mm (Table 1). Meanwhile, picosecond laser treatments using an MLA-type handpiece at the wavelength of 1064 nm were delivered

Table 1 Settings for 532-nm picosecond-domain neodymium:yttrium–aluminum–garnet (Nd:YAG) laser treatment using an MLA-type beam on ex vivo human skin

Spot size (mm)	Average fluence (J/cm^2)	Average power density (W/cm^2)	Power density of microbeam (W/cm^2)		Pass
			Distance of 31 mm*	Distance of 48 mm*	
6	1.0	2.22×10^9	4.49×10^{11}	1.12×10^{11}	1

*The distance between the microlens and the surface of the skin

with a spot size of 7 mm, a laser fluence of 1.9 J/cm^2, and a distance step of 31 mm over a single pass using single-pulse and dual-pulse modes (Table 2). Additionally, 1064-nm MLA-type, picosecond laser treatments were delivered with a 4-mm spot size and laser fluence of 2.8 J/cm^2 over a single pass using single-pulse and dual-pulse modes. Finally, MLA-type laser treatments at the wavelength of 1064 nm were delivered with a spot size of 10 mm and laser fluence of 0.3 J/cm^2 over five passes using single-pulse and dual-pulse modes.

Histopathological and immunohistochemical studies

Human tissue samples for each treatment setting were obtained 30 min after treatment, collecting the epidermis, dermis, and subcutaneous fat. The tissue samples were fixed in 10% buffered formalin and embedded in paraffin. Then, serial tissue sections, which were cut along the longitudinal plane at a thickness of 5 μm for each condition, were prepared and stained with hematoxylin and eosin.

Additionally, tissue sections from the ex vivo human skin were subjected to immunohistochemical staining for CD31 and Melan-A. Briefly, slides were incubated with rabbit anti-CD31 polyclonal antibody (ab28364; Abcam; Abcam, Cambridge, UK) at a dilution of 1:50 and with rabbit anti-Melan-A monoclonal antibody (ab210546) at a dilution of 1:500, respectively, as primary antibodies. They were further incubated with a secondary antibody (REAL™ EnVision™ HRP Rabbit/Mouse Detection System; DAKO) for 30 min at room temperature. Then, sections were developed with 3,3′-diaminobenzidine chromogen and counterstained with hematoxylin. Negative controls were obtained by omitting the primary antibody.

Histometric measurement and statistical analysis

The sizes of laser-induced cystic cavitation zones were evaluated by measuring mean widths and heights thereof using ImageJ software (version 1.48; National Institutes of Health, Bethesda, MD, USA). Estimated values of the widths and heights are presented as a mean ± standard deviation. A normality test was performed using the Kolmogorov–Smirnov test, and the results were analyzed via a two-independent-sample *t* test by parametric criteria using SAS software (Version 9.2; SAS Institute, Inc., Cay, NC, USA). Differences with *P* values of less than 0.05 were considered statistically significant.

Results

Microlens array-type, 532-nm picosecond-domain laser-induced tissue reactions

Immediately after a single pulse of 532-nm picosecond laser treatment on ex vivo human skin at the distance step of 31 mm, the fractionated appearance of cystic cavitation lesions with a cavitation size of 83.4 ± 16.5 μm × 70.2 ± 17.3 μm was found in the basilar layer of the epidermis (Fig. 1a, b). Meanwhile, at the 48-mm distance step, cystic cavitation lesions with a size of 91.0 ± 44.7 μm × 81.2 ± 36.3 μm were found in the lower epidermis and upper papillary dermis (Fig. 1c, d). Additionally, microscopic perinuclear vacuolar changes were also found in the lower epidermis and upper papillary dermis around the areas of cystic cavitation in both settings. The difference in the sizes of cystic cavitation between the distance steps of 31 mm and 48 mm was statistically insignificant ($P > 0.05$). Nonetheless, the location of cystic cavitation was deeper in the epidermis and dermis, and the area of microscopic vacuolization was wider at the 48-mm distance step, compared to 31 mm.

Immunoreactivity for CD31 and Melan-A in 532-nm MLA-type laser treatment

Immunohistochemical stain for the panvascular marker CD31 at both the 31-nm and 48-nm distance settings exhibited CD31-positive microvascular components with intact structural integrity in the dermis (Fig. 2a). Most of the cystic cavitation and microscopic perinuclear vacuolization underneath the basement membrane zone was negative for CD31 immunostaining; however, a few areas of CD31-positive cystic cavitation were found in the upper papillary dermis (Fig. 2b). Meanwhile, immunohistochemical stain for Melan-A at both the 31-nm and 48-nm distance settings revealed that epidermal cystic cavitation contained one or two Melan-A-positive cells (Fig.

Table 2 Settings for 1064-nm picosecond-domain Nd:YAG laser treatment using an MLA-type beam on ex vivo human skin at a distance step of 31 mm

Spot size (mm)	Average fluence (J/cm^2)	Average power density (W/cm^2)	Power density of microbeam (W/cm^2)	Pass
4	2.8	6.22×10^9	7.04×10^{11}	1
7	1.9	4.22×10^9	4.78×10^{11}	1
10	0.3	6.67×10^8	7.55×10^{10}	5

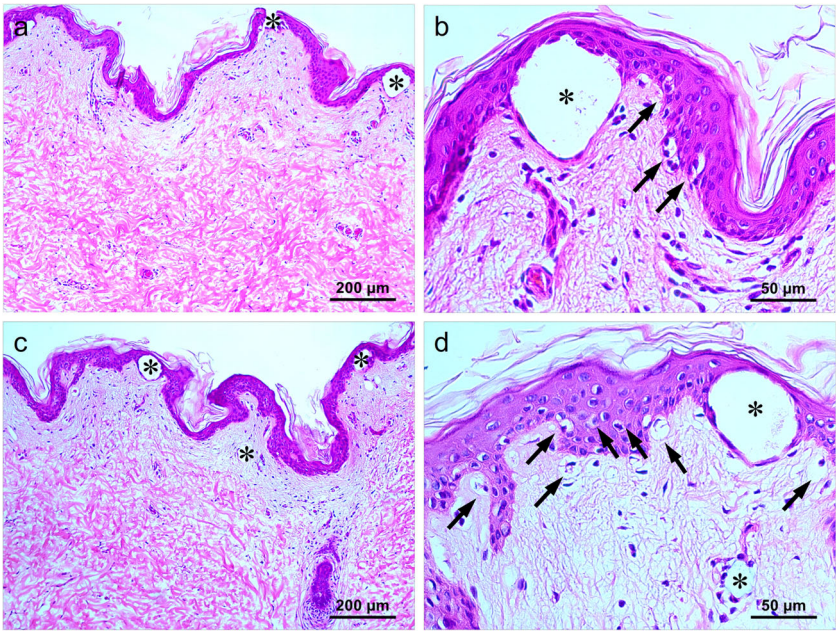

Fig. 1 Tissue reactions after 532-nm microlens array (MLA)-type, picosecond laser treatment. Single-pulse, 532-nm picosecond laser treatment at a 6-mm spot size and a fluence of 1.0 J/cm^2 generated the fractionated appearance of cystic cavitation lesions (asterisks) in the lower epidermis and papillary dermis. Microscopic perinuclear vacuolar changes (arrows) were found around cystic cavitation. Distance between the microlens and the skin of **a**, **b** 31 mm and **c**, **d** 48 mm. H&E stain at **a**, **c** original magnification × 100 and **b**, **d** × 400

2c–f). However, cellular components in the dermal cystic cavitation were negative for Melan-A immunostaining. Moreover, no remarkable Melan-A-positive cells were found in the dermis of both experimental settings.

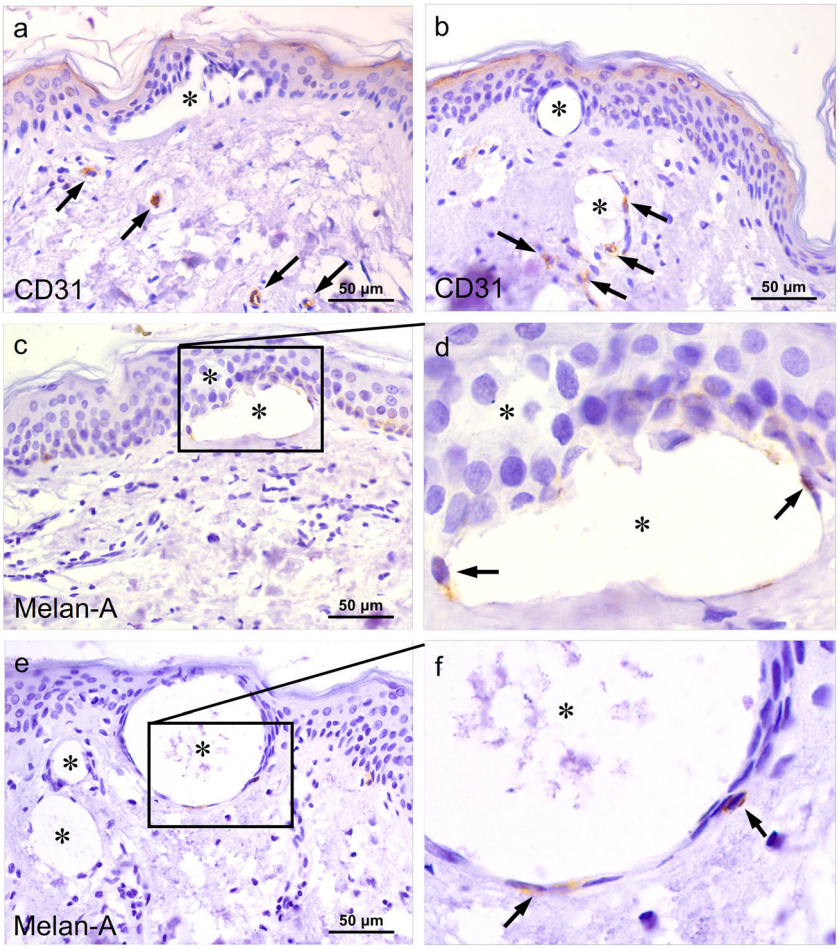

Fig. 2 Immunohistochemical staining for CD31 and Melan-A after 532-nm MLA-type, picosecond laser treatment. Single-pulse, 532-nm picosecond laser treatment at a 6-mm spot size and a fluence of 1.0 J/cm^2 generated cystic cavitation lesions (asterisks) in the lower epidermis and papillary dermis. **a** CD31-positive dermal microvascular components with intact structural integrity (arrows). **b** CD31-positive dermal microvascular components in association with cystic cavitation (arrows). **c–f** Melan-A-positive lining cells of epidermal cystic cavitation lesions (arrows). Distance between the microlens and the skin of **a**, **c**, **d** 31 mm and **b**, **e**, **f** 48 mm. **a**, **b** CD31 immunohistochemical stain. **c–f** Melan-A immunohistochemical stain. **a**, **b**, **c**, **e** Original magnification × 400

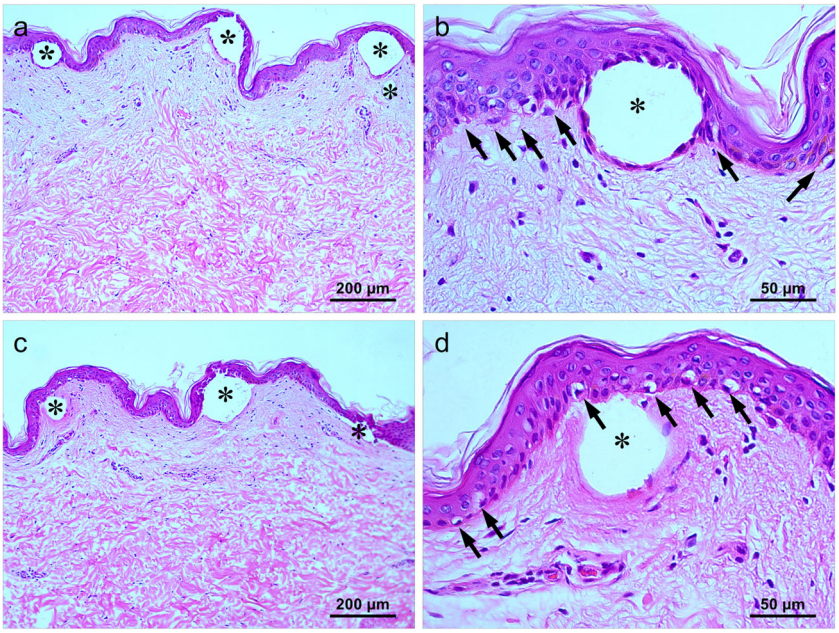

Fig. 3 Tissue reactions after 1064-nm MLA-type, picosecond laser treatment. Single-pulse, 1064-nm picosecond laser treatment at a 7-mm spot size and a fluence of 1.9 J/cm^2 generated the fractionated appearance of cystic cavitation lesions (asterisks) throughout the lower epidermis and upper papillary dermis at regular intervals. Microscopic perinuclear vacuolar changes (arrows) were found around the areas of cystic cavitation. **a**, **b** Single-pulse mode and **c**, **d** dual-pulse mode treatment. H&E stain at original magnification **a**, **c** × 100 and **b**, **d** × 400

Microlens array-type, 1064-nm picosecond-domain laser-induced tissue reaction

Immediately after a single pulse on ex vivo human skin at a 7-mm spot size and laser fluence of 1.9 J/cm^2, the fractionated appearance of cystic cavitation zones with a size of 107.0 ± 18.1 μm × 83.3 ± 37.4 μm was found in the basilar epidermis or basement membrane zone and upper papillary dermis at regular intervals (Fig. 3a, b). Meanwhile, picosecond laser treatment in the dual-pulse mode generated cystic cavitation zones with a size of 100.8 ± 40.4 μm × 83.1 ± 29.4 μm in the deeper part of the epidermis or dermis (Fig. 3c, d). However, the difference in the sizes of cystic cavitation between the pulse modes was statistically insignificant ($P > 0.05$). In both

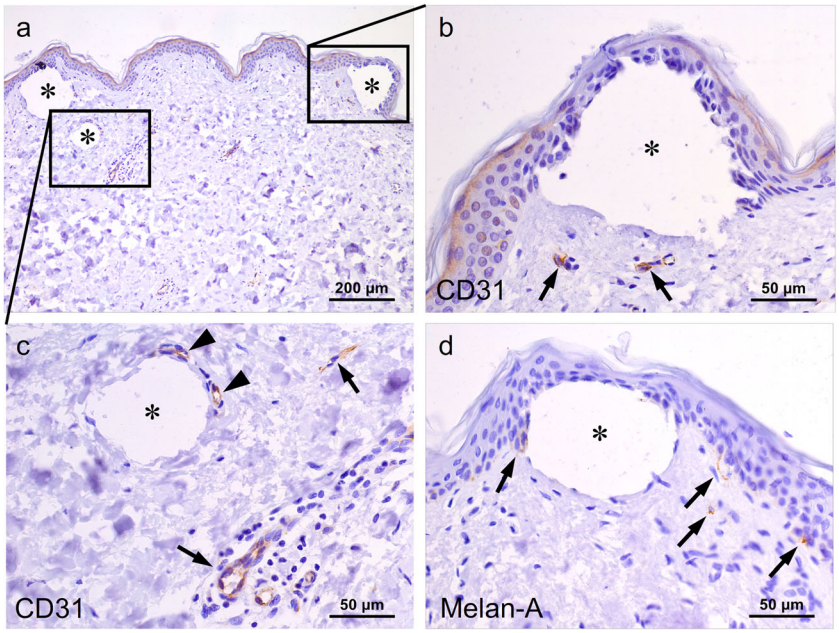

Fig. 4 Immunohistochemical staining for CD31 and Melan-A after 1064-nm MLA-type, picosecond laser treatment. **a** Single-pulse, 1064-nm picosecond laser treatment at a 7-mm spot size, a fluence of 1.9 J/cm^2 generated cystic cavitation lesions (asterisks) in the lower epidermis and papillary dermis. **b** CD31-positive dermal microvascular components with intact structural integrity (arrows). **c** CD31-positive dermal microvascular components with intact structural integrity (arrows) and CD31-positive microvascular cells in association with cystic cavitation (arrowheads). **d** Melan-A-positive cells in the lining cells of epidermal cystic cavitation and basilar epidermis (arrows). **a**–**c** CD31 immunohistochemical stain. **d** Melan-A immunohistochemical stain. Original magnification **a** × 100 and **b**–**d** × 400

pulse modes, microscopic perinuclear vacuolization was found in the lower epidermis and upper papillary dermis around the areas of cystic cavitation, although somewhat less remarkably than that with 532-nm laser treatment.

Immunoreactivity for CD31 and Melan-A in 1064-nm MLA-type laser treatment

Immunohistochemical stain for CD31 after treatment in the sing-pulse mode at a 7-mm spot size and laser fluence of 1.9 J/cm^2 revealed a few cystic cavitation lesions in the dermis, but not in the epidermis and basement membrane zone, with CD31-positive microvascular components (Fig. 4a–c). Immunohistochemical stain for Melan-A showed that the lining cells of the cystic cavitation areas in the epidermis, but not in the dermis, contained Melan-A-positive cells; a few Melan-A-positive cells were also found in the dermis (Fig. 4d). Meanwhile, dual-pulse irradiation at a 7-mm spot size and laser fluence of 1.9 J/cm^2 elicited Melan-A-positive, CD31-negative cystic cavitation in the epidermis without noticeable CD31-positive, and Melan-A-negative cystic lesions in the dermis (data not shown). Furthermore, none of the dermal components exhibited remarkable immunoreactivity to Melan-A staining (data not shown).

A single pulse at a high-power density versus multiple pulses at a low-power density

In the single- and dual-pulse modes, 1064-nm MLA-type, picosecond laser treatment at a 4-mm spot size and a laser fluence of 2.8 J/cm^2 generated patterns of cavitation and vacuolization formation similar to those generated at a 7-mm spot size and laser fluence of 1.9 J/cm^2 (Fig. 5a, b). Both single- and dual-pulse irradiation at a 4-mm spot size and a laser fluence of 2.8 J/cm^2 elicited Melan-A-positive, CD31-negative cystic cavitation in the epidermis and noticeable CD31-positive, Melan-A-negative cystic lesions in the dermis (Fig. 5c–f). Furthermore, a few discrete Melan-A-positive cells were also found in the dermis for both the single- and dual-pulse modes.

The experimental settings of a 10-mm spot size, 0.3-J/cm^2 fluence, and five passes appeared to generate microscopic vacuolar changes widely distributed throughout the lower epidermis and upper papillary dermis without remarkable cystic cavitation formation for both the single- and dual-pulse modes

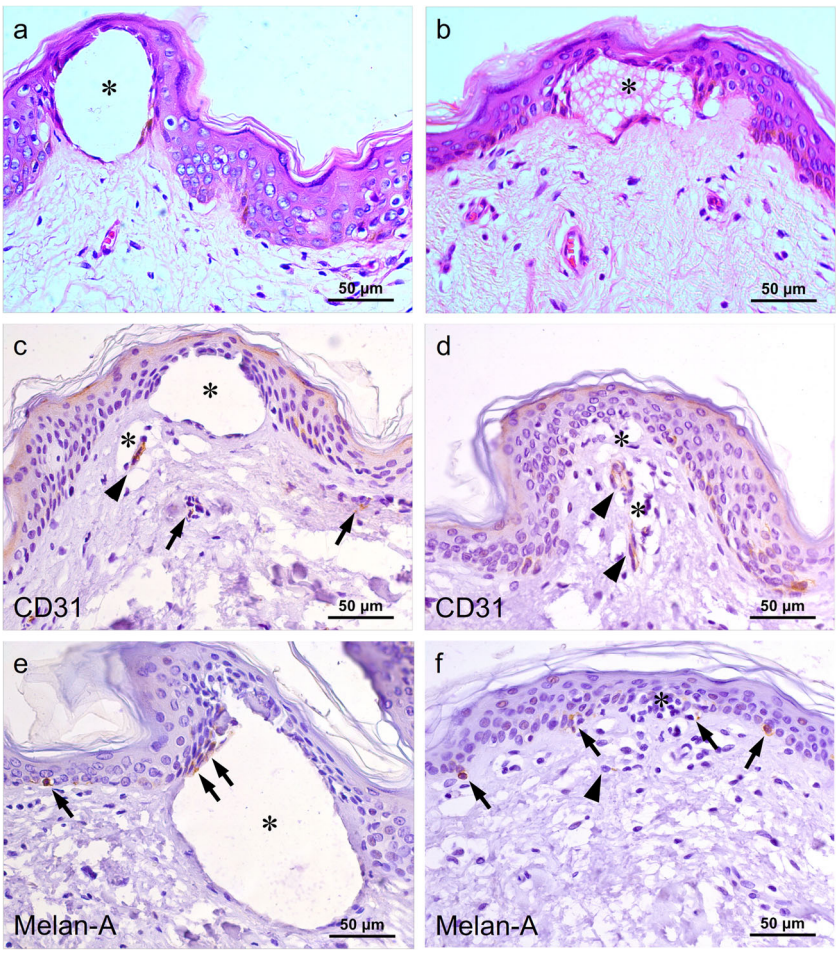

Fig. 5 Tissue reactions after 1064-nm picosecond laser treatment at high-power density. **a–f** Single-pulse, 1064-nm picosecond laser treatment at a 4-mm spot size and a fluence of 2.8 J/cm^2 generated cystic cavitation lesions (asterisks) in the lower epidermis and upper papillary dermis. **c**, **d** CD31-positive dermal microvascular components with intact structural integrity (arrows) and CD31-positive microvascular cells in association with cystic cavitation (arrowheads). **e** Melan-A-positive cells in the lining cells of epidermal cystic cavitation and basilar epidermis (arrows). **f** Melan-A-positive cells in the basilar epidermis with or without perinuclear vacuolization (arrows) and in the dermis (arrowhead). **a**, **c**, **e** Single-pulse mode and **b**, **d**, **f** dual-pulse mode treatment. **a**, **b** H&E stain. **c**, **d** CD31 immunohistochemical stain. **e**, **f** Melan-A immunohistochemical stain. Original magnification × 400

(Fig. 6a, b). Melan-A-positive cells in the upper papillary dermis were more readily observed with the single-pulse mode, compared to the dual-pulse mode (Fig. 6c–f). Dermal cells with microscopic perinuclear vacuolization were nonreactive to CD31 immunostaining (data not shown).

Discussion

In this study, we microscopically analyzed ex vivo the patterns of 532- and 1064-nm picosecond laser-induced tissue reactions in Asian skin. Herein, an MLA-type optic array was used to generate high-intensity micro-injury zones in the epidermis and dermis. The histopathological data in this study revealed distinguished zones of cystic cavitation and perinuclear vacuolization throughout the lower epidermis and upper papillary dermis. Most of the cystic tissue reactions in the epidermis appeared to be dependent on the absorption properties of chromophores and presented CD31-negative/Melan-A-positive immunoreactivity in the lining cells of the cystic cavities. Meanwhile, the laser-induced cystic cavitation lesions in the dermis exhibited three different patterns of CD31/Melan-A immunoreactivity: (1) CD31-positive/Melan-A-negative lining cells of the cystic cavities, (2) CD31-negative/Melan-A-negative cystic cavitation without lining cells near uninjured CD31-positive/Melan-A-negative microvascular components, and (3) CD31-negative/Melan-A-negative cystic cavitation without adjacent microvascular components. Additionally, most of the CD31-positive/Melan-A-negative or CD31-negative/Melan-A-negative dermal cystic lesions were markedly smaller in size, compared to CD31-negative/Melan-A-positive epidermal cavitation lesions.

The microbeams utilized in our study had a power density lower than the irradiation threshold for initiating multiphoton absorption (~10^{13} W/cm^2 in water) and for generating seed electrons [8]. Thus, although the precise initiation mechanism for producing seed electrons still remains to be elucidated, we deemed that chromophore-dependent thermionic emission by picosecond laser pulses likely contributed to generating laser-induced tissue breakdown in our ex vivo human skin study. The location, size, and density of the areas of cystic cavitation and perinuclear vacuolization seemed to correlate with the power density and the concentration of pigment chromophores and also appeared to be inversely correlated with the

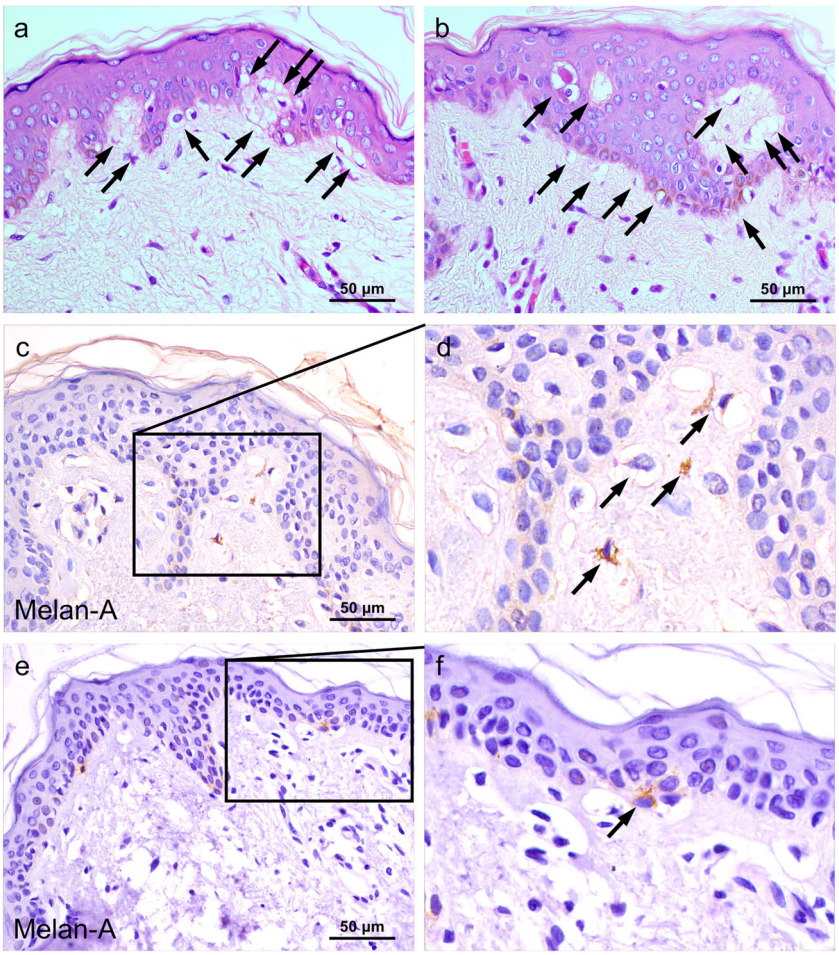

Fig. 6 Tissue reactions after multiple pulses of 1064-nm picosecond laser treatment. **a**, **b** Five passes of 1064-nm picosecond laser treatment at a 10-mm spot size and a fluence of 0.3 J/cm^2 generated microscopic perinuclear vacuolization (arrows) widely distributed throughout the lower epidermis and upper papillary dermis. **c**, **d** Melan-A-positive cells in the basilar epidermis and upper papillary dermis (arrows). **e**, **f** Melan-A-positive cells in the basilar epidermis (arrow). **a**, **c**, **d** Single-pulse mode and **b**, **e**, **f** dual-pulse mode treatment. **a**, **b** H&E stain. **c**–**f** Melan-A immunohistochemical stain. **a**, **b**, **c**, **e** Original magnification × 400

depth of pigments and vascular components as a result of a loss of laser energy due to tissue scattering. Nonetheless, our data demonstrated that cystic cavitation lesions in the dermis can be generated both in microvascular components, collagen bundles, and perivascular loose connective tissue and that dermal cystic cavitation lesions could be generated somewhat independent of the absorption properties of chromophores. Accordingly, we also suggest that chromophore-dependent tissue breakdown by thermionic emission could have affected the irradiation threshold for developing chromophore-independent tissue breakdown in the dermis. Notwithstanding, although the distance between the grids for each experimental setting was at least 0.5 cm, the possibilities of picosecond-domain laser-induced photothermal and photoacoustic effects on the other areas could not be completely excluded.

Dual-pulse delivery of Nd:YAG laser pulses have been used for treating various pigmentary disorders by irradiating energy to target tissues in split fluence at dual-pulse intervals in the nanosecond to microsecond range [10–12]. Dual-pulse treatments using Q-switched Nd:YAG lasers have been described as reducing the risk of side effects and as increasing the clinical efficacy thereof, compared to single-pulse treatments, particularly in Asian patients [11, 12]. A previous simulation study using a black tattoo-embedded, bovine serum albumin-polyacrylamide hydrogel phantom demonstrated that split-fluence delivery of laser pulses broke tattoo particles into more homogeneous granules, compared to single-pulse delivery [13]. Also, photothermal vacuolar formation in the surrounding tissue was less remarkable with a dual-pulse mode than with a single-pulse mode [13]. In the present study, dual-pulse treatments consisted of two consecutive, half-fluenced, 450-ps pulses at 1.5-ns intervals. The 1.5-ns pulse interval between the two half-fluenced pulses in the dual-pulse mode was determined by considering the half-life of the plasma and when the density of the plasma decayed to 1/e [14]. Herein, compared to single-pulse irradiation, dual-pulse irradiation more effectively generated cystic cavitation zones in the ex vivo skin. Moreover, with the repetitive delivery of picosecond laser pulses in the dual-pulse mode, fewer Melan-A-positive cells were found, compared to laser delivery in the single-pulse mode.

Research suggests that the plasma induced in the skin upon laser emission expands in the direction opposite to the irradiation axis during the laser pulse by absorbing remaining energy and preventing the penetration of the laser deeper into the tissue [13]. Picosecond-domain laser treatment at a higher power density generates the plasma and associated tissue reactions in the upper part of target tissue [13]. In light of the results of this study, we deemed that, in the dual-pulse mode, the first of the two half-fluenced, 450-ps pulses may have decreased the shielding effects of the laser-induced plasma by lowering the power density. Meanwhile, the second half-fluenced pulse may have effectively increased the volume and density of the plasma in the target tissue.

Conclusion

Our microscopic findings in ex vivo human skin demonstrated that 532- and 1064-nm picosecond-domain Nd:YAG laser treatments generate fractionated zones of cystic cavitation and perinuclear vacuolization throughout the lower epidermis and upper papillary dermis. Immunohistochemical staining for the panvascular marker CD31 and Melan-A revealed that the zones of cystic cavitation and microscopic perinuclear vacuolization in the epidermis were negative for CD31 and positive for Melan-A. Meanwhile, dermal laser-induced tissue breakdown areas exhibited various features of immunoreactivity against CD31 and Melan-A that included CD31-positive and Melan-A-negative, CD31-negative and Melan-A-positive, and/or CD31-negative and Melan-A-negative patterns according to the various treatment settings. Although further in vivo human skin study is needed to confirm our findings, we believe that our histopathologic and immunohistopathologic investigations may help with predicting MLA-type, picosecond-domain laser-induced tissue reactions for treating skin lesions in Asian patients.

Acknowledgements We would like to thank Anthony Thomas Milliken, ELS (Editing Synthase, Seoul, Korea) for his help with the editing of this manuscript.

Funding This study was supported by research funding from Lutronic Corporation. The funding company had no role in the study design, data collection, data analysis, manuscript preparation, or publication. The authors have indicated no significant interest with commercial supporters

Compliance with ethical standards This study was approved by the Institutional Review Board of International St. Mary's Hospital, Catholic Kwandong University College of Medicine.

Conflict of interest The authors declare that they have no conflict of interest.

References

1. Balu M, Lentsch G, Korta DZ, König K, Kelly KM, Tromberg BJ, Zachary CB (2017) In vivo multiphoton-microscopy of picosecond-laser-induced optical breakdown in human skin. Lasers Surg Med 49:555–562
2. Tanghetti EA (2016) The histology of skin treated with a picosecond alexandrite laser and a fractional lens array. Lasers Surg Med 48:646–652
3. Tanghetti E, Jennings J (2018) A comparative study with a 755 nm picosecond alexandrite laser with a diffractive lens array and a 532 nm/1064 nm Nd:YAG with a holographic optic. Lasers Surg Med 50:37–44
4. Brauer JA, Kazlouskaya V, Alabdulrazzaq H, Bae YS, Bernstein LJ, Anolik R, Heller PA, Geronemus RG (2015) Use of a

picosecond pulse duration laser with specialized optic for treatment of facial acne scarring. JAMA Dermatol 151:278–284
5. Werner S, Krieg T, Smola H (2007) Keratinocyte-fibroblast interactions in wound healing. J Invest Dermatol 127:998–1008
6. Orringer JS, Rittié L, Hamilton T, Karimipour DJ, Voorhees JJ, Fisher GJ (2011) Intraepidermal erbium: YAG laser resurfacing: impact on the dermal matrix. J Am Acad Dermatol 64:119–128
7. Bernstein EF, Schomacker KT, Basilavecchio LD, Plugis JM, Bhawalkar JD (2017) Treatment of acne scarring with a novel fractionated, dual-wavelength, picosecond-domain laser incorporating a novel holographic beam-splitter. Lasers Surg Med 49:796–802
8. Varghese B, Bonito V, Jurna M, Palero J, Verhagen MH (2015) Influence of absorption induced thermal initiation pathway on irradiance threshold for laser induced breakdown. Biomed Opt Express 6:1234–1240
9. Lee HC, Chang DW, Lee EJ, Yoon HW (2017) High-energy, subnanosecond linearly polarized passively Q-switched MOPA laser system. Opt Laser Technol 95:81–85
10. Goo BL, Kang JS, Cho SB (2015) Treatment of early-stage erythematotelangiectatic rosacea with a Q-switched 595-nm Nd:YAG laser. J Cosmet Laser Ther 17:139–142
11. Kim BW, Lee MH, Chang SE, Yun WJ, Won CH, Lee MW, Choi JH, Moon KC (2013) Clinical efficacy of the dual-pulsed Q-switched neodymium:yttrium-aluminum-garnet laser: comparison with conservative mode. J Cosmet Laser Ther 15:340–341
12. Ahn KJ, Kim BJ, Cho SB (2017) Simulation of laser-tattoo pigment interaction in a tissue-mimicking phantom using Q-switched and long-pulsed lasers. Skin Res Technol 23:376–383
13. Vogel A, Busch S, Jungnickel K, Birngruber R (1994) Mechanisms of intraocular photodisruption with picosecond and nanosecond laser pulses. Lasers Surg Med 15:32–43
14. Docchio F (1988) Lifetimes of plasmas induced in liquids and ocular media by single Nd:YAG laser pulses of different duration. Europhys Lett 6:407–412